The Astrophysical Journal Letters, 743:L14 (6pp), 2011 December 10 doi:10.1088/2041-8205/743/1/L14

FIRST SEARCH FOR POINT SOURCES OF HIGH-ENERGY COSMIC NEUTRINOS WITH THE ANTARES NEUTRINO TELESCOPE*

S. Adrián-Martínez[1], J. A. Aguilar[2], I. Al Samarai[3], A. Albert[4], M. André[5], M. Anghinolfi[6], G. Anton[7], S. Anvar[8], M. Ardid[1], A. C. Assis Jesus[9], T. Astraatmadja[9,38], J.-J. Aubert[3], B. Baret[10], S. Basa[11], V. Bertin[3], S. Biagi[12,13], A. Bigi[14], C. Bigongiari[2], C. Bogazzi[9], M. Bou-Cabo[1], B. Bouhou[10], M. C. Bouwhuis[9], J. Brunner[3,39], J. Busto[3], F. Camarena[1], A. Capone[15,16], C. Cârloganu[17], G. Carminati[12,13,40], J. Carr[3], S. Cecchini[12], Z. Charif[3], Ph. Charvis[18], T. Chiarusi[12], M. Circella[19], R. Coniglione[20], H. Costantini[3,6], P. Coyle[3], C. Curtil[3], M. P. Decowski[9], I. Dekeyser[21], A. Deschamps[18], C. Distefano[20], C. Donzaud[10,22], D. Dornic[2], Q. Dorosti[23], D. Drouhin[4], T. Eberl[7], U. Emanuele[2], A. Enzenhöfer[7], J.-P. Ernenwein[3], S. Escoffier[3], P. Fermani[15,16], M. Ferri[1], V. Flaminio[14,24], F. Folger[7], U. Fritsch[7], J.-L. Fuda[21], S. Galatà[3], P. Gay[17], G. Giacomelli[12,13], V. Giordano[20], J. P. Gómez-González[2], K. Graf[7], G. Guillard[17], G. Halladjian[3], G. Hallewell[3], H. van Haren[25], J. Hartman[9], A. J. Heijboer[9], Y. Hello[18], J. J. Hernández-Rey[2], B. Herold[7], J. Hößl[7], C. C. Hsu[9], M. de Jong[9,38], M. Kadler[26], O. Kalekin[7], A. Kappes[7], U. Katz[7], O. Kavatsyuk[23], P. Kooijman[9,27,28], C. Kopper[7,9], A. Kouchner[10], I. Kreykenbohm[26], V. Kulikovskiy[6,29], R. Lahmann[7], P. Lamare[8], G. Larosa[1], D. Lattuada[20], D. Lefèvre[21], G. Lim[9,28,40], D. Lo Presti[30,31], H. Loehner[23], S. Loucatos[32], S. Mangano[2], M. Marcelin[11], A. Margiotta[12,13], J. A. Martínez-Mora[1], A. Meli[7], T. Montaruli[19,33], L. Moscoso[10,32,41], H. Motz[7], M. Neff[7], E. Nezri[11], D. Palioselitis[9], G. E. Păvălaş[34], K. Payet[32], P. Payre[3,41], J. Petrovic[9], P. Piattelli[20], N. Picot-Clemente[3], V. Popa[34], T. Pradier[35], E. Presani[9], C. Racca[4], C. Reed[9], C. Richardt[7], R. Richter[7], C. Rivière[3], A. Robert[21], K. Roensch[7], A. Rostovtsev[36], J. Ruiz-Rivas[2], M. Rujoiu[34], G. V. Russo[30,31], F. Salesa[2], D. F. E. Samtleben[9], P. Sapienza[20], F. Schöck[7], J.-P. Schuller[32], F. Schüssler[32], T. Seitz[7], R. Shanidze[7], F. Simeone[15,16], A. Spies[7], M. Spurio[12,13], J. J. M. Steijger[9], Th. Stolarczyk[32], A. Sánchez-Losa[2], M. Taiuti[6,37], C. Tamburini[21], S. Toscano[2], B. Vallage[32], V. Van Elewyck[10], G. Vannoni[32], M. Vecchi[3], P. Vernin[32], S. Wagner[7], G. Wijnker[9], J. Wilms[26], E. de Wolf[9,28], H. Yepes[2], D. Zaborov[36], J. D. Zornoza[2], and J. Zúñiga[2]

[1] Institut d'Investigació per a la Gestió Integrada de les Zones Costaneres (IGIC), Universitat Politècnica de València, C/Paranimf 1, 46730 Gandia, Spain
[2] IFIC-Instituto de Física Corpuscular, Edificios Investigación de Paterna, CSIC, Universitat de València, Apdo. de Correos 22085, 46071 Valencia, Spain
[3] CPPM, Aix-Marseille Université, CNRS/IN2P3, Marseille, France
[4] GRPHE-Institut universitaire de technologie de Colmar, 34 rue du Grillenbreit BP 50568–68008 Colmar, France
[5] Technical University of Catalonia, Laboratory of Applied Bioacoustics, Rambla Exposició, 08800 Vilanova i la Geltrú, Barcelona, Spain
[6] INFN-Sezione di Genova, Via Dodecaneso 33, 16146 Genova, Italy
[7] Friedrich-Alexander-Universität Erlangen-Nürnberg, Erlangen Centre for Astroparticle Physics, Erwin-Rommel-Str. 1, 91058 Erlangen, Germany
[8] Direction des Sciences de la Matière, Institut de recherche sur les lois fondamentales de l'Univers, Service d'Electronique des Détecteurs et d'Informatique, CEA Saclay, 91191 Gif-sur-Yvette Cedex, France
[9] Nikhef, Science Park, Amsterdam, The Netherlands
[10] APC-Laboratoire AstroParticule et Cosmologie, UMR 7164 (CNRS, Université Paris 7 Diderot, CEA, Observatoire de Paris) 10, rue Alice Domon et Léonie Duquet 75205 Paris Cedex 13, France
[11] LAM-Laboratoire d'Astrophysique de Marseille, Pôle de l'Étoile Site de Château-Gombert, rue Frédéric Joliot-Curie 38, 13388 Marseille Cedex 13, France
[12] INFN-Sezione di Bologna, Viale C. Berti-Pichat 6/2, 40127 Bologna, Italy
[13] Dipartimento di Fisica dell'Università, Viale Berti Pichat 6/2, 40127 Bologna, Italy
[14] INFN-Sezione di Pisa, Largo B. Pontecorvo 3, 56127 Pisa, Italy
[15] INFN-Sezione di Roma, P. le Aldo Moro 2, 00185 Roma, Italy
[16] Dipartimento di Fisica dell'Università La Sapienza, P. le Aldo Moro 2, 00185 Roma, Italy
[17] Clermont Université, Université Blaise Pascal, CNRS/IN2P3, Laboratoire de Physique Corpusculaire, BP 10448, 63000 Clermont-Ferrand, France
[18] Géoazur-Université de Nice Sophia-Antipolis, CNRS/INSU, IRD, Observatoire de la Côte d'Azur and Université Pierre et Marie Curie, BP 48, 06235 Villefranche-sur-mer, France
[19] INFN-Sezione di Bari, Via E. Orabona 4, 70126 Bari, Italy
[20] INFN-Laboratori Nazionali del Sud (LNS), Via S. Sofia 62, 95123 Catania, Italy
[21] COM-Centre d'Océanologie de Marseille, CNRS/INSU et Université de la Méditerranée, 163 Avenue de Luminy, Case 901, 13288 Marseille Cedex 9, France
[22] Univ Paris-Sud, 91405 Orsay Cedex, France
[23] Kernfysisch Versneller Instituut (KVI), University of Groningen, Zernikelaan 25, 9747 AA Groningen, The Netherlands
[24] Dipartimento di Fisica dell'Università, Largo B. Pontecorvo 3, 56127 Pisa, Italy
[25] Royal Netherlands Institute for Sea Research (NIOZ), Landsdiep 4,1797 SZ 't Horntje (Texel), The Netherlands
[26] Dr. Remeis-Sternwarte and ECAP, Universität Erlangen-Nürnberg, Sternwartstr. 7, 96049 Bamberg, Germany
[27] Universiteit Utrecht, Faculteit Betawetenschappen, Princetonplein 5, 3584 CC Utrecht, The Netherlands
[28] Universiteit van Amsterdam, Instituut voor Hoge-Energie Fysika, Science Park 105, 1098 XG Amsterdam, The Netherlands
[29] Moscow State University, Skobeltsyn Institute of Nuclear Physics, Leninskie gory, 119991 Moscow, Russia
[30] INFN-Sezione di Catania, Viale Andrea Doria 6, 95125 Catania, Italy
[31] Dipartimento di Fisica ed Astronomia dell'Università, Viale Andrea Doria 6, 95125 Catania, Italy
[32] Direction des Sciences de la Matière, Institut de recherche sur les lois fondamentales de l'Univers, Service de Physique des Particules, CEA Saclay, 91191 Gif-sur-Yvette Cedex, France
[33] Department of Physics, University of Wisconsin, Madison, 53706 WI, USA
[34] Institute for Space Sciences, R-77125 Bucharest, Măgurele, Romania
[35] IPHC-Institut Pluridisciplinaire Hubert Curien, Université de Strasbourg et CNRS/IN2P3 23 rue du Loess, BP 28, 67037 Strasbourg Cedex 2, France
[36] ITEP-Institute for Theoretical and Experimental Physics, B. Cheremushkinskaya 25, 117218 Moscow, Russia
[37] Dipartimento di Fisica dell'Università, Via Dodecaneso 33, 16146 Genova, Italy
Received 2011 July 31; accepted 2011 October 11; published 2011 November 21

ABSTRACT

Results are presented of a search for cosmic sources of high-energy neutrinos with the ANTARES neutrino telescope. The data were collected during 2007 and 2008 using detector configurations containing between 5 and 12 detection lines. The integrated live time of the analyzed data is 304 days. Muon tracks are reconstructed using a likelihood-based algorithm. Studies of the detector timing indicate a median angular resolution of 0.5 ± 0.1 deg. The neutrino flux sensitivity is $7.5 \times 10^{-8} (E_\nu / \mathrm{GeV})^{-2}\ \mathrm{GeV}^{-1}\ \mathrm{s}^{-1}\ \mathrm{cm}^{-2}$ for the part of the sky that is always visible ($\delta < -48$ deg), which is better than limits obtained by previous experiments. No cosmic neutrino sources have been observed.

Key words: astroparticle physics – cosmic rays – neutrinos

Online-only material: color figures

1. INTRODUCTION

High-energy cosmic rays permeate the universe, but their origins remain uncertain. Many types of acceleration sites have been suggested, such as supernova remnants, micro-quasars, and active galactic nuclei (see, e.g., Becker 2008 for a review).

If such objects are sources of cosmic rays, high-energy neutrinos may also be produced. These may be detected as a diffuse flux (Aguilar et al. 2011b), but the observation of point-like sources of cosmic neutrinos would offer a unique opportunity to identify and study the sites and mechanisms of cosmic-ray acceleration.

In this Letter, results are presented of a search for cosmic point-like sources of high-energy muon neutrinos performed with the first data taken by the ANTARES telescope. Located in the Mediterranean Sea, the ANTARES experiment is predominantly sensitive to neutrinos from the southern hemisphere in the TeV to PeV energy range. In particular, this allows the study of Galactic sources and complements the IceCube observatory, which primarily explores the northern hemisphere.

2. DATA COLLECTION

The detection principle relies on measuring Cherenkov light emitted by high-energy-charged particles that result from neutrino interactions inside or near the instrumented volume. In particular, charged current interactions of muon–neutrinos produce high-energy muons. The muon direction closely follows that of the neutrino and can often be reconstructed with sub-degree accuracy. The large background from downgoing muons due to cosmic-ray interactions in the atmosphere is reduced by selecting only upgoing muons as neutrino candidates.

The Cherenkov light is detected by an array of photomultiplier tubes (PMT), each housed in a pressure-resistant glass sphere called an Optical Module (OM; Amram et al. 2002). The OMs are placed in storeys of triplets separated by 14.5 m along vertical detector lines, which are anchored to the seabed at a depth of 2475 m. The line spacing is approximately 60 m. Lines 1 through 11 (line 12) contain 25 (20) storeys for a total of 875 OMs.

The arrival time and charge of the photomultiplier signals are digitized (Aguilar et al. 2010b) into "hits" and transmitted to shore. An online filter identifies events containing muons within the data stream which otherwise consists of optical backgrounds due to natural radioactive decays and bioluminescence. The selected events are stored for offline reconstruction. Detailed descriptions of the detector, the data acquisition, and the online filtering algorithms are given in Ageron et al. (2011) and Aguilar et al. (2007).

2.1. Data Taking and Processing

The data presented here were collected between 2007 January 31 and 2008 December 30. During this time, the construction of the ANTARES detector was still in progress. The detector consisted of 5 lines for most of 2007 and of 9, 10, and 12 detector lines during 2008. The total live time of the data used for the analysis is 304 days (144, 38, 48, and 74 days with 5, 9, 10, and 12 detector lines, respectively.)

The online event selection identifies triplets of OMs that detect multiple photons, either as a high-charge hit or as hits separated by less than 20 ns on adjacent OMs. At least four such triplets are required throughout the detector, with the relative photon arrival times being compatible with the hypothesis that light is emitted along the track of a relativistic particle.

The arrival times of the hits are calibrated as described in Aguilar et al. (2011a). The inter-line timing has been measured in an iterative procedure by comparing the expected hit times to those measured in a large sample of reconstructed downgoing muons. Compatible results were obtained using the calibration system consisting of pulsed laser and LED beacons to measure the relative timing delays.

The positions and orientations of the OMs vary because of the sea currents. An acoustic positioning system, combined with compasses and tiltmeters located along the detector lines, measures the positions and orientations of the OMs, with an accuracy of $\sim$10 cm.

2.2. Event Reconstruction and Selection

From the timing and position information of the hits, muon tracks are reconstructed using a multi-stage fitting procedure (Heijboer 2004). The initial fitting stages provide the hit selection and starting point for the final fit. The final stage consists of a fit of the likelihood $\mathcal{L}$ to the observed hit times and includes the contribution of optical background hits. Several starting points of the procedure are tried to increase the probability of finding the global likelihood maximum. The reconstruction quality of the final track is quantified by a parameter $\Lambda = \mathcal{L}^{\mathrm{final}}/N_{\mathrm{dof}} + 0.1(N_{\mathrm{conv}} - 1)$, where $N_{\mathrm{dof}} = N_{\mathrm{hits}} - 5$ is the number of degrees of freedom in the fit, and N_{conv} is the number of starting points that converged to the same final fit. The second term in the Λ definition is an ad hoc reward for fits with $N_{\mathrm{conv}} > 1$.

* We dedicate this Letter to the memory of our colleague and friend Luciano Moscoso, who passed away during the preparation of this Letter.

[38] Also at University of Leiden, the Netherlands.

[39] On leave at DESY, Platanenallee 6, D-15738 Zeuthen, Germany.

[40] Now at University of California, Irvine, 92697 CA, USA.

[41] Deceased.

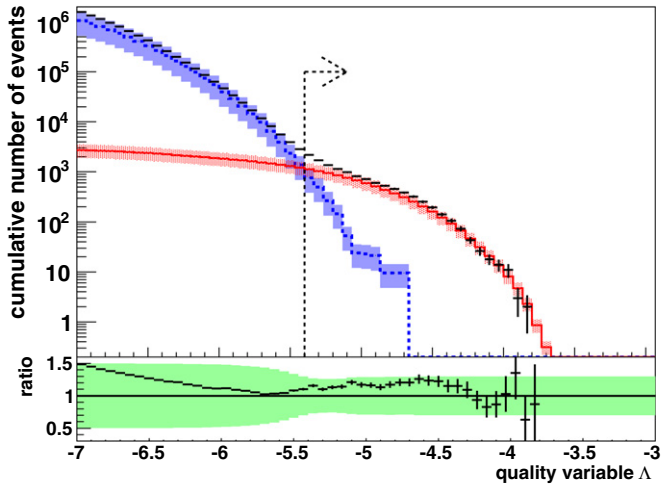

Figure 1. Cumulative distribution of the reconstruction quality variable, Λ, for upgoing events in data (black points) that have an error estimate <1 deg. The Monte Carlo simulated contributions from mis-reconstructed atmospheric muons (dashed blue line) and from atmospheric neutrinos (solid red line) are also shown. The bottom panel shows the ratio between data and simulation. The shaded regions indicate the uncertainties on the simulation. The vertical line indicates the analysis cut $\Lambda > -5.4$.

(A color version of this figure is available in the online journal.)

Neutrino candidates are selected from upgoing events using criteria that have been determined in a "blind" manner, i.e., before performing the search analysis on the data. The criteria are chosen to optimize the expected median value of the upper limit on the neutrino flux (i.e., sensitivity).

The angular uncertainty obtained from the likelihood fit of the muon track is required to be smaller than 1 deg. This cut removes 75% of the upward reconstructed atmospheric muons.

The cumulative distribution of Λ for muons that are reconstructed as upgoing is shown in Figure 1 along with the simulated contributions from atmospheric muons and neutrinos. The simulation uses Agrawal et al. (1996) for the atmospheric neutrino flux; see Barr et al. (2006) for the flux uncertainty. The atmospheric muons are simulated by the QGSJET (Kalmykov & Ostapchenko 1993) and CORSIKA (Heck et al. 1998) packages with the primary cosmic-ray flux from Nikolsky et al. (1984). Comparisons between different simulation chains resulted in a muon flux uncertainty of 50% (Aguilar et al. 2010a).

The final sample of neutrino candidates consists of 2190 upgoing events with $\Lambda > -5.4$ and an angular uncertainty <1 deg. This is compatible with the simulation, which predicts 763 ± 381 muon and 1130 ± 339 neutrino events to pass these cuts, for a total of 1893 ± 509. Hence, the sample is expected to consist of about 60% atmospheric neutrinos and 40% misreconstructed muons.

3. DETECTOR PERFORMANCE

The angular resolution and effective area of the detector for neutrinos passing the selection cuts have been determined using simulations and are shown in Figure 2. The simulations include the stochastic energy loss of muons via electromagnetic shower production, the propagation of Cherenkov photons through sea water, and a detailed simulation of the detector electronics.

3.1. Angular Resolution

The cumulative distribution of the angle between the reconstructed muon direction and the neutrino direction is shown in Figure 2 (left panel) for neutrino events with a neutrino spectrum proportional to E_ν^{-2}, where E_ν is the neutrino energy. The median of this angular error is 0.5 ± 0.1 deg. For the subset of data in which the full 12 line detector was operational, the resolution is estimated to be 0.4 ± 0.1 deg.

While the deficit of atmospheric muons caused by the Moon shadow is currently observed by ANTARES at the 2.7σ level (Rivière 2011), significantly more data are required to stringently constrain the angular resolution. Instead, the systematic uncertainty on this quantity has been estimated by varying the time resolution of the OMs Δ_t in the simulation. The allowed range of Δ_t is determined by requiring that the resulting simulated number of neutrino events, as determined by selecting events in the neutrino dominated region, $\Lambda > -5$, be compatible with the number observed in data. The best agreement between

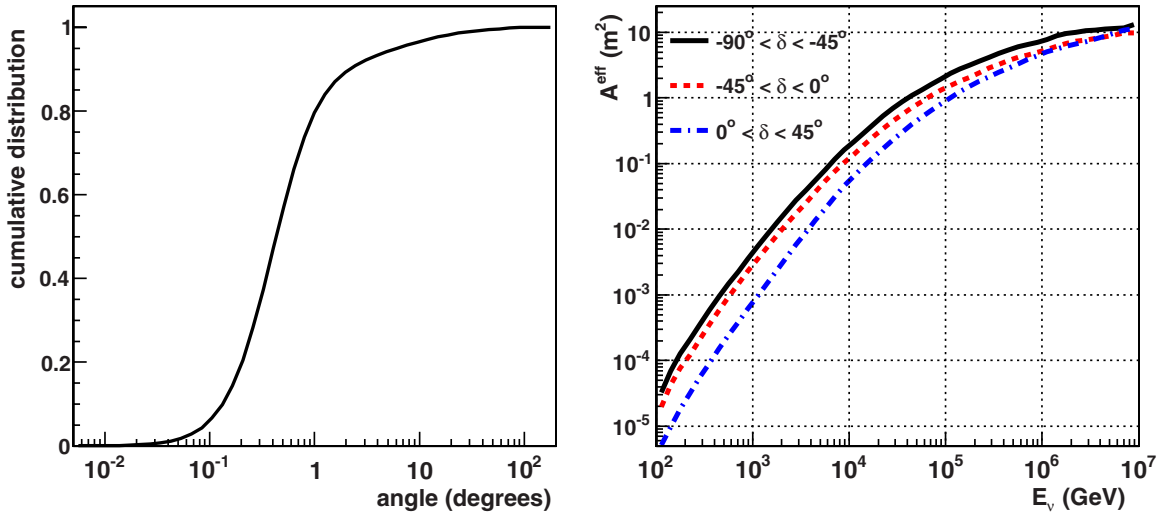

Figure 2. Performance of the detector for the selected signal events as determined from simulation. The cumulative distribution of the angle between the reconstructed muon direction and the true neutrino direction is shown for selected signal events with an E_ν^{-2} spectrum (left panel). The neutrino effective area $A_\nu^{\rm eff}$, averaged over three declination ranges, is shown as a function of the neutrino energy (right panel).

(A color version of this figure is available in the online journal.)

data and simulation is obtained for $\Delta_t = 2.5$ ns, which is somewhat larger than the nominal expected resolution of 1.5 ns. Hence, this value is used for all simulations in this analysis, in particular for extracting the central value of the allowed range of angular resolutions. For a simulated timing resolution of 3.4 ns, the number of observed neutrinos exceeds the simulation by 60%, which is twice the amount allowed by the systematic neutrino flux uncertainty of 30% (Barr et al. 2006). This discrepancy thus places a 2σ upper bound on the time resolution, which translates into a 1σ systematic uncertainty on the angular resolution of 0.1 deg. This uncertainty incorporates, to first order, all effects which have a net result of degrading the time resolution, such as possible mis-alignments of the detector, inaccuracies in the simulation of light propagation in the water or in the transit time distribution of the PMT. A similar analysis with analogous results has been performed using downgoing muon data instead of upgoing neutrino candidates.

The absolute orientation of the detector is known with an accuracy of about 0.1 deg (Halladjian 2010); this uncertainty is taken into account as an independent effect.

3.2. Acceptance

The effective area for muon neutrinos $A_\nu^{\rm eff}$ is defined as the ratio between the selected neutrino event rate and the cosmic neutrino flux. It is determined from simulations and is shown in Figure 2 (right panel) as a function of the neutrino energy for three declination intervals. Throughout this Letter, the cosmic neutrino flux is assumed to consist of an equal amount of ν_μ and $\bar{\nu}_\mu$.

In the search, limits are set on the constant ϕ in the flux parameterization $dN/dE_\nu = \phi \times [E_\nu/\mathrm{GeV}]^{-2}\,\mathrm{GeV}^{-1}\,\mathrm{cm}^{-2}\,\mathrm{s}^{-1}$. The acceptance A for such a flux is defined as the constant of proportionality between the number of selected signal events and the flux intensity ϕ. It can be computed by convoluting $A_\nu^{\rm eff}(E)$ with $dN/dE_\nu(E)$. For declinations $\delta < -48$ deg, A and $A_\nu^{\rm eff}$ are approximately constant in declination. For -48 deg $< \delta < 48$ deg, the functions decrease because of the requirement that the tracks are upgoing. For a source declination of -90 (0) deg, $A = 3.2$ (1.8) $\times 10^7$ GeV cm^2 s. This means a total of 3.2(1.8) neutrinos would be detected and selected from a point source with a flux of 10^{-7} GeV^{-1} cm^{-2} s^{-1}. For this flux model, the energy of 80% of the selected signal is in the range 3 TeV $< E_\nu <$ 700 TeV.

To constrain the systematic uncertainty on the acceptance, the atmospheric neutrino data have been compared to a simulation in which the efficiency of each OM is reduced. A 15% effect was observed, which is applied as the systematic uncertainty on the acceptance in the limit calculations.

4. SEARCH METHOD

Two distinct approaches to look for point-like neutrino sources have been used. In the *full-sky search*, a search is made for an excess of events over the atmospheric neutrino background anywhere in the field of view. In addition, a *candidate list search* is made, where the presence of a signal is tested at the locations of 24 pre-defined high-energy gamma-ray sources that could be expected to emit neutrinos. They include supernova remnants, microquasars, and BL Lac objects. While more restrictive in scope, the candidate list search requires less signal to reach a significant excess, compared to the all-sky search.

4.1. Event Likelihood

The search method is based on the likelihood of observing the events, defined as

$$\log \mathcal{L}_{\rm s+b} = \sum_i \log[\mu_{\rm sig} \times \mathcal{F}(\beta_i(\delta_s, \alpha_s)) + \mathcal{B}(\delta_i)] - \mu_{\rm sig} - N_{\rm bg}, \quad (1)$$

where the sum is over the neutrino candidate events, and $\mathcal{F}$ is a parameterization of the point-spread function. This is defined as the probability density to find the reconstructed muon i an angle β away from the declination δ_s and right ascension α_s of the source; it is closely related to the angular resolution (see Figure 2). $\mathcal{B}(\delta)$ is a smooth parameterization of the background rate derived from the observed declination distribution of the 2190 selected events. The mean number of selected signal events produced by the source is $\mu_{\rm sig}$. The term $N_{\rm bg}$ represents the total number of expected background events, which is constant and therefore does not influence the maximum-likelihood fits or the likelihood ratio.

In the candidate list search, the likelihood is maximized for each candidate by numerically fitting the source intensity $\mu_{\rm sig}$ to the events located within 20 deg of the source, with the source coordinates fixed to the known position. In the full-sky search, potentially significant clusters are first identified using a loose cone selection, which requires at least four events in a cone of 3 deg diameter. For each cluster, the likelihood is maximized by fitting the source coordinates and the intensity, yielding maximum-likelihood estimates for these quantities.

The next step is to compute the test statistic, which is defined as the logarithm of the likelihood ratio:

$$Q = \log \mathcal{L}_{\rm s+b}^{\rm max} - \log \mathcal{L}_{\rm b}, \quad (2)$$

where $\mathcal{L}_{\rm s+b}^{\rm max}$ is the maximum value of the likelihood found in the fit and $\mathcal{L}_{\rm b}$ is the likelihood computed for the background-only hypothesis ($\mu_{\rm sig} = 0$). A large (small) value of Q indicates that the data are compatible with the signal (background).

4.2. Statistical Interpretation

Pseudo-experiments are generated by randomly sampling the declination from the background parameterization $\mathcal{B}$ and the right ascension from a uniform distribution. Events from a neutrino point source are added and distributed around the desired coordinates according to the point-spread function. The systematic uncertainties on the angular resolution and orientation of the detector are incorporated by varying the simulated characteristics of the signal events within the assigned uncertainties.

Distributions of Q obtained by applying the search method to the pseudo-experiments are used to extract p-values and limits corresponding to the observed Q in the data. The limits are obtained following Feldman & Cousins (1998).

5. RESULTS

Figure 3 shows a sky map of the selected events in equatorial coordinates along with the locations of sources from the candidate list (circles) and of the most significant cluster found in the full-sky search (square).

No significant clusters of neutrino candidates have been found in either search.

In the full-sky search, the most signal-like cluster has a fitted source position $(\alpha_s, \delta_s) = (43.^\circ21, -0.^\circ50)$. The fit assigns

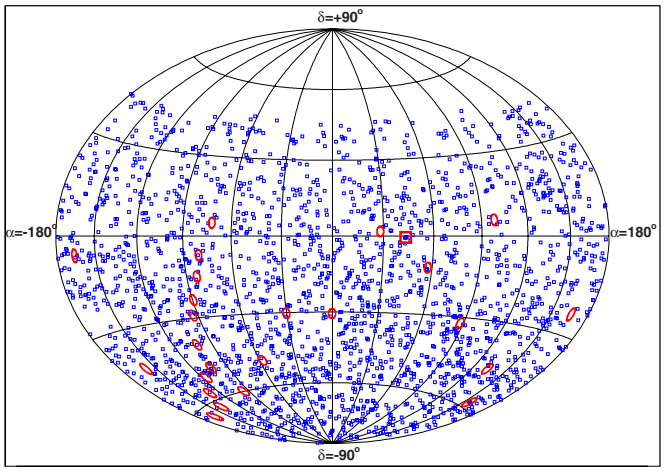

Figure 3. Map in equatorial coordinates of the 2190 selected neutrino candidates. The position of the most significant cluster (see the text) is indicated by the square. The circles denote the positions of the 24 sources from the candidate list.

(A color version of this figure is available in the online journal.)

Table 1
Results of the Candidate List Search

Source	α_s (deg)	δ_s (deg)	$\mu_{\rm sig}^{\rm fit}$	Q	p-Value	$\phi^{90\%\rm CL}$
HESS J1023-575	155.83	−57.76	2.7	2.5	0.17	2.0
GX 339	−104.30	−48.79	2.2	2.1	0.26	1.9
RX J1713.7-3946	−101.75	−39.75	1.0	1.7	0.46	2.2
HESS J1837-069	−80.59	−6.95	1.1	1.5	0.55	2.6
1ES 0347-121	57.35	−11.99	1.4	1.1	0.70	2.5
3C 279	−165.95	−5.79	0.91	0.74	0.83	2.4
Cir X-1	−129.83	−57.17	0.82	0.65	0.85	1.5
PKS 2005-489	−57.63	−48.82	0	0	...	1.1
Galactic Center	−93.58	−29.01	0	0	...	1.2
LS 5039	−83.44	−14.83	0	0	...	1.4
H 2356-309	−0.22	−30.63	0	0	...	1.1
RX J0852.0-4622	133.00	−46.37	0	0	...	0.76
PKS 0548-322	87.67	−32.27	0	0	...	1.1
PSR B1259-63	−164.30	−63.83	0	0	...	0.76
PKS 2155-304	−30.28	−30.22	0	0	...	1.0
HESS J1614-518	−116.42	−51.82	0	0	...	0.59
SS 433	−72.04	4.98	0	0	...	1.1
HESS J0632+057	98.24	5.81	0	0	...	1.2
RCW 86	−139.32	−62.48	0	0	...	0.47
RGB J0152+017	28.17	1.79	0	0	...	0.89
Centaurus A	−158.64	−43.02	0	0	...	0.49
ESO 139-G12	−95.59	−59.94	0	0	...	0.36
W28	−89.57	−23.34	0	0	...	0.61
1ES 1101-232	165.91	−23.49	0	0	...	0.61

Notes. The source coordinates and the Q and p-values are shown as well as the limits on the E_ν^{-2} flux intensity $\phi^{90\%\rm CL}$; the latter has units 10^{-7} GeV^{-1} cm^{-2} s^{-1}. The rows are sorted in order of increasing p-value.

3.4 events as signal events and finds $Q = 6.8$. Such a value, or larger (more signal like), occurs with a probability[42] $p = 88\%$ anywhere in the field of view.

The results of the candidate list search are shown in Table 1. The most signal-like source candidate is HESS J1023-575, where three(five) events are within 1(3) deg of its position. For this cluster of events, $Q = 2.5$. In the absence of a signal such a value or larger has a probability of $p = 17\%$ to occur among the 24 source candidates.

[42] The p-values quoted refer to the individual searches, without a "trial" factor for the fact that two searches were conducted.

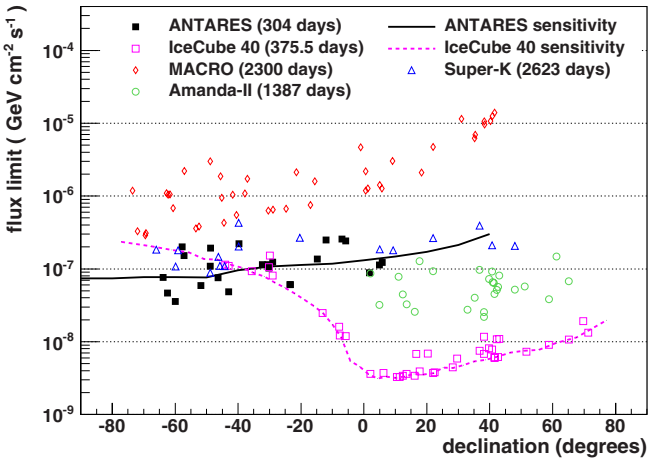

Figure 4. Limits set on the normalization ϕ of an E_ν^{-2} spectrum of high-energy neutrinos from selected candidates (see Table 1). The points show the 90% CL limit at the declination of the candidate source. In addition to the present result, several previously published limits on sources in both the southern and northern hemisphere are shown from Ambrosio et al. (2001), Thrane et al. (2009), Abbasi et al. (2009), and Abbasi et al. (2011). Also shown are sensitivities (solid and dashed lines) for the current analysis and for the search from Abbasi et al. (2011) (see Abbasi et al. 2009; Thrane et al. 2009 for the sensitivities corresponding to those searches).

(A color version of this figure is available in the online journal.)

5.1. Neutrino Flux Upper Limits

As no significant point sources are observed, 90% confidence level limits are obtained for the intensity, $\phi^{90\%\rm CL}$, of an E_ν^{-2} neutrino flux from each of the source candidates. They are listed in Table 1 and are shown in Figure 4 as a function of the source declination. Figure 4 also shows the sensitivity of this analysis. It is in agreement with the median value of the actually observed limits. For the area of the sky that is always visible ($\delta < -48$ deg), the sensitivity is about $7.5 \times 10^{-8} (E_\nu/\rm GeV)^{-2}\,\rm GeV^{-1}\,s^{-1}\,cm^{-2}$.

The present limits are more stringent than those obtained for the northern hemisphere by previous multi year experiments (also indicated in the figure) and are competitive with those set by the IceCube collaboration (Abbasi et al. 2011) for $\delta < -30$ deg. It should be noted that even though each experiment sets limits on the intensity of an assumed E_ν^{-2} spectrum, the experiments are sensitive in different energy ranges. For this spectrum, ANTARES detects most events at energies in a broad range around 10 TeV, which is the relevant energy range for several galactic sources (Crocker et al. 2005). Southern hemisphere limits shown from the IceCube experiment probe the neutrino flux predominantly in the region above 1 PeV (Abbasi et al. 2011).

The event selection and the search method have been cross-checked with an independent analysis using the same selection criteria and a search method based on the expectation-maximization algorithm (Dempster et al. 1977; Aguilar & Hernandez-Rey 2008). In this method, the angular spread of the signal events is a free parameter in the likelihood and the maximization is performed analytically. The results of both the full-sky and the candidate list search are consistent with the results discussed earlier.

6. AUTOCORRELATION ANALYSIS

In a separate analysis, the cumulative distribution of the number of event pairs as a function of their angular separation has been studied using the neutrino candidate events. This autocorrelation analysis has been employed to search for features in the data such as an excess of tracks at an arbitrary level of angular separation. The study is independent of detector simulations and neutrino source models.

A reference autocorrelation distribution is determined by scrambling the data itself approximately one million times and averaging the resulting distributions. The comparison between the data and the reference distribution is performed following Li & Ma (1983).

The maximum excess above the reference distribution has a significance of 1.1σ at angular scales smaller than 7 deg. Such a deviation is expected from a collection of random background events with a (trial factor corrected) probability of 55%.

7. CONCLUSIONS

A search for cosmic sources of high-energy neutrinos using the data taken with the ANTARES neutrino telescope during the first two years of operation has been presented. For the first half of the data considered, the detector was about half its final size. An estimate of the angular resolution constrained by data yields 0.5 ± 0.1 deg (0.4 deg for the 12 line detector), confirming the expectation that excellent angular resolution is achievable using sea water as the detection medium. Neither the full-sky search nor the candidate list search shows a significant excess of events. Limits have been obtained on the high-energy neutrino flux for a number of selected source candidates. For many candidate sources, the limits presented here are the most stringent to date.

The authors acknowledge the financial support of the funding agencies: Centre National de la Recherche Scientifique (CNRS), Commissariat á l'énergie atomique et aux énergies alternatives (CEA), Agence National de la Recherche (ANR), Commission Européenne (FEDER fund and Marie Curie Program), Région Alsace (contrat CPER), Région Provence-Alpes-Côte d'Azur, Département du Var and Ville de La Seyne-sur-Mer, France; Bundesministerium für Bildung und Forschung (BMBF), Germany; Istituto Nazionale di Fisica Nucleare (INFN), Italy; Stichting voor Fundamenteel Onderzoek der Materie (FOM), Nederlandse organisatie voor Wetenschappelijk Onderzoek (NWO), the Netherlands; Council of the President of the Russian Federation for young scientists and leading scientific schools supporting grants, Russia; National Authority for Scientific Research (ANCS), Romania; Ministerio de Ciencia e Innovación (MICINN), Prometeo of Generalitat Valenciana and MultiDark, Spain. We also acknowledge the technical support of Ifremer, AIM and Foselev Marine for the sea operation, and the CC-IN2P3 for the computing facilities.

REFERENCES

Abbasi, R., Abdou, Y., Abu-Zayyad, T., et al. 2011, ApJ, 732, 18
Abbasi, R., Ackermann, M., Adams, J., et al. 2009, Phys. Rev. D, 79, 062001
Ageron, M., et al. 2011, Nucl. Instrum. Methods, A656, 11
Agrawal, V., Gaisser, T. K., Lipari, P., & Stanev, T. 1996, Phys. Rev. D, 53, 1314
Aguilar, J. A., & Hernandez-Rey, J. J. 2008, Astropart. Phys., 29, 117
Aguilar, J. A., Albert, A., Ameli, F., et al. 2007, Nucl. Instrum. Methods, A570, 107
Aguilar, J. A., Albert, A., Anton, G., et al. 2010a, Astropart. Phys., 34, 179
Aguilar, J. A., Al Samarai, I., Albert, A., et al. 2010b, Nucl. Instrum. Methods, A622, 59
Aguilar, J. A., Al Samarai, I., Albert, A., et al. 2011a, Astropart. Phys., 34, 539
Aguilar, J. A., Samarai, I. Al, Albert, A., et al. 2011b, Phys. Lett. B, 696, 16
Ambrosio, M., Antolini, R., Auriemma, G., et al. 2001, ApJ, 546, 1038
Amram, P., Anghinolfi, M., Anvar, S., et al. 2002, Nucl. Instrum. Methods A, 484, 369
Barr, G. D., Gaisser, T. K., Robbins, S., & Stanev, T. 2006, Phys. Rev. D, 74, 094009
Becker, J. K. 2008, Phys. Rep., 458, 173
Crocker, R. M., Melia, F., & Volkas., R. R. 2005, ApJ, 622, L37
Dempster, A. P., Laird, N. M., & Rubin, D. B. 1977, R. Stat. Soc. Ser. B, 39, 1
Feldman, G. J., & Cousins, R. D. 1998, Phys. Rev. D, 57, 3873
Halladjian., G. 2010, PhD thesis, Université de la Méditérranée-Aix Marseille II
Heck, D., et al. 1998, *CORSIKA:* A Monte Carlo Code to Simulate Extensive Air Showers, Forschungszentrum Karlsruhe Rep. FZKA 6019, http://www.ik.fzk.de/corsika/physics_description/corsika_phys.html
Heijboer, A. J. 2004, PhD thesis, Universiteit van Amsterdam
Kalmykov, N. N., & Ostapchenko, S. S. 1993, Phys. At. Nuclei, 56, 346
Li, T. P., & Ma, Y. Q. 1983, ApJ, 272, 317
Nikolsky, S. I., Stamenov, I. N., & Ushev, S. Z. 1984, Sov. Phys.—JETP, 60, 10
Rivière, C. 2011, Proc. 32nd ICRC (Beijing), in press
Thrane, E., Abe, K., Hayato, Y., et al. 2009, ApJ, 704, 503